Biomed Microdevices (2016) 18: 63
DOI 10.1007/s10544-016-0090-y

A simple microfluidic device to study cell-scale endothelial mechanotransduction

Julie Lafaurie-Janvore[1] · **Elizabeth E. Antoine**[1] · **Sidney J. Perkins**[1,2] · **Avin Babataheri**[1] · **Abdul I. Barakat**[1]

Published online: 12 July 2016

Abstract Atherosclerosis is triggered by chronic inflammation of arterial endothelial cells (ECs). Because atherosclerosis develops preferentially in regions where blood flow is disturbed and where ECs have a cuboidal morphology, the interplay between EC shape and mechanotransduction events is of primary interest. In this work we present a simple microfluidic device to study relationships between cell shape and EC response to fluid shear stress. Adhesive micropatterns are used to non-invasively control EC elongation and orientation at both the monolayer and single cell levels. The micropatterned substrate is coupled to a microfluidic chamber that allows precise control of the flow field, high-resolution live-cell imaging during flow experiments, and *in situ* immunostaining. Using micro particle image velocimetry, we show that cells within the chamber alter the local flow field so that the shear stress on the cell surface is significantly higher than the wall shear stress in regions containing no cells. In response to flow, we observe the formation of lamellipodia in the downstream portion of the EC and cell retraction in the upstream portion. We quantify flow-induced calcium mobilization at the single cell level for cells cultured on unpatterned surfaces or on adhesive lines oriented either parallel or orthogonal to the flow. Finally, we demonstrate flow-induced intracellular calcium waves and show that the direction of propagation of these waves is determined by cell polarization rather than by the flow direction. The combined versatility and simplicity of this microfluidic device renders it very useful for studying relationships between EC shape and mechanosensitivity.

Keywords Atherosclerosis · Mechanobiology · Shear stress · Calcium signaling · Micropatterns · Microfluidic flow chamber

1 Introduction

Atherosclerosis, the disease that leads to heart attacks and strokes, develops preferentially at arterial branches and bifurcations where blood flow is multi-directional and highly disturbed (Chien 2007; Hahn and Schwartz 2009). Atherosclerosis is also fundamentally a disease that involves dysfunction of the endothelium, the cellular monolayer lining the inner surfaces of blood vessels. Thus, elucidating the role that arterial blood flow plays in the development of the disease requires understanding endothelial cell (EC) mechanotransduction, i.e. how ECs sense and transmit mechanical forces and how they transduce these forces into biochemical signals that modulate cellular function and dysfunction. In particular, flow-derived shear stress is a key regulator of EC functions including vasomotion, maintenance of vascular permeability, and the expression of inflammatory and adhesive proteins (Chatzizisis et al. 2007; Li et al. 2005).

The shear stress field within medium and large arteries prone to atherosclerosis is complex and highly dynamic (Barakat 2013). Although most studies have focused on the global large-scale shear stress within arteries, shear stress at the more local scale of individual cells is the more relevant

Electronic supplementary material The online version of this article (doi:10.1007/s10544-016-0090-y) contains supplementary material, which is available to authorized users.

✉ Abdul I. Barakat
barakat@ladhyx.polytechnique.fr

[1] Laboratoire d'Hydrodynamique de l'École polytechnique, CNRS-EP UMR 7646, Palaiseau, France

[2] Columbia University, New York, NY, USA

parameter for understanding EC mechanotransduction because it directly reflects the mechanical microenvironment to which the cells are exposed (Yurdagul et al. 2016). Computational simulations have predicted that the wavy nature of the EC surface alters the local shear stress on the cell surface and leads to large subcellular shear stress gradients (Barbee et al. 1995; Satcher et al. 1992). This is particularly significant in light of data demonstrating EC sensitivity to such gradients (DePaola et al. 1999). The simulations also suggested that flow-induced EC elongation and alignment in the direction of flow leads to a reduction in subcellular shear stress gradients and may thus constitute a form of structural adaptation of the cells to the imposed flow (Li et al. 2005). A recent modeling study from our group suggested that the dynamics of endothelial responsiveness to flow are determined not only by the magnitude of the shear stress on the cell surface but also by the orientation of the stress exerted by the fluid relative to the major axis of the cell (Gouget et al., 2015). These observations of connections between EC shape, orientation, and sensitivity to flow are particularly interesting in light of the fact that atherosclerosis *in vivo* initiates in arterial regions where ECs are cuboidal (round) whereas zones where ECs are elongated remain largely spared (Davies 1995). Therefore, probing relations among EC shape, flow-derived mechanical forces and predilection for atherosclerosis requires experimental platforms that simultaneously enable control of EC shape, exposure of the cells to controlled flow environments, measurement of shear stress with subcellular resolution, control of the relative orientation between the cells and the applied forces, and real-time imaging of cellular responses. The present work describes one such platform.

Previous studies have described a variety of microfluidic devices that offer control of flow and geometric parameters as well as surface characteristics to mimic physiological conditions (Shemesh et al. 2015; Polacheck et al. 2013; Young and Simmons 2010) and enable investigation of biological responses (Chan et al. 2015). The current tendency is towards the development of increasingly elaborate and sophisticated systems that capture many features of the *in vivo* microenvironment. A prominent example is the development of organ-on-a-chip platforms (An et al. 2015; Beebe et al. 2013). In the present work, our goal was to devise a simple system that allows exploration of the interplay between EC shape and mechanotransduction with subcellular-scale precision. To this end, we present a simple-to-implement and easy-to-use flow chamber that allows independent control of cell shape and flow-induced shear stress as well as high-resolution live-cell imaging (in phase contrast or fluorescence) during flow. EC shape control is accomplished at either the monolayer or single-cell level by using adhesive micropatterns of different dimensions, thus allowing the study of either collective or single cell behavior. The micropatterned substrate is coupled to a microfluidic chamber that allows precise control of the flow field and therefore regulation of the shear stress exerted by the flow on the ECs. Some systems that combine flow, substrate microfabrication, and live-cell imaging exist (Lin and Helmke 2012; Hsu et al. 2005; Wang et al. 2011; Lam et al. 2014); however, they do not provide a sufficiently high resolution to measure the flow microenvironment and to dynamically monitor biological events at a subcellular level while simultaneously controlling intracellular organization via micropatterns. We use our new system to characterize the global shear stress in the chamber as well as the local shear stress around individual cells using micro particle image velocimetry (PIV). We also investigate various EC biological responses to flow including cell polarization, whole-cell calcium mobilization, and subcellular calcium wave propagation.

2 Materials and methods

2.1 Surface micropatterning

Surface micropatterns on glass coverslips were fabricated using the deep UV protein micropatterning method described previously (Azioune et al. 2010). Briefly, 24 × 60 mm #1 glass coverslips were cleaned with ethanol and activated by 1 min exposure to O_2 plasma (Harrick) before being incubated for 1 h with 0.1 mg/mL poly-L-lysine-g-poly(ethyleneglycol) (PLL(20)-g[3.5]-PEG(2), SuSoS) in 10 mM HEPES at pH 7.3 for passivation. After washing with distilled water, the treated surface was illuminated with deep UV light (UVO Cleaner; Jelight) through a chromium synthetic quartz photomask (Toppan). After assembly of the microfluidic chamber (see below), the surface was treated for 1 h with a 50 μg/ml bovine fibronectin (Sigma Aldrich) solution in phosphate-buffered saline (PBS; Gibco, Invitrogen), rinsed with PBS and kept overnight at 4 °C. Rhodamine-conjugated fibronectin (Cytoskeleton) was used to produce fluorescent micropatterns.

2.2 Microfluidic system and flow control

To produce the top surface of the chamber, ~1 mm-diameter holes were drilled through a regular microscope glass slide using a sand blaster. Polydimethylsiloxane (PDMS; Sylgard 184, Dow-Corning) plugs containing holes for the inlet and outlet were then covalently bonded to the slide using plasma activation of both the PDMS plugs and the glass slide. To form the flow chamber, double-sided tape (Orafol) was cut using a high precision cutting plotter (Graphtec), and the microfluidic device was assembled by embedding the double-sided tape between the prepared glass slide (top) and either a regular or a micropatterned glass coverslip (bottom). The use of hollow PDMS plugs over small holes in the glass slide ensured

robust, leak-free connections with inlet and outlet steel pins attached to platinum-cured silicone tubing (0.5 mm inner diameter; Fisher Scientific). After assembly, the device was treated with fibronectin and seeded with cells (see below). For fibronectin coating, washing steps, cell seeding and cell culture, all liquid handling was performed by manual syringe aspiration of fluid through the flow chamber rather than positive-pressure flow. This method was used in order to minimize air bubble formation in the device. As the chamber is minimally gas-permeable, fresh medium was intermittently aspirated through the chamber during the 3 h of cell culture before the flow experiments. For flow experiments, a syringe pump (Harvard Apparatus) was used to deliver complete cell culture medium (see next paragraph) at a prescribed constant flow rate of 1.8 mL/min.

2.3 Cell culture, cell seeding and immunostaining

Primary bovine aortic endothelial cells (BAECs; passages 5–10) were cultured at 37 °C and 5 % CO_2 in Dulbecco's Modified Eagle's Medium (DMEM; Gibco) supplemented with 10 % fetal bovine serum (Gibco) and 1 % penicillin/streptomycin (Gibco). After fibronectin coating of the device, the cells were seeded in the microfluidic chamber. This was accomplished by detaching the cells from cell culture flasks by trypsinization and concentrating them by centrifugation to obtain a solution containing 5 million cells/mL which was aspirated into the chamber. After 1 h incubation to allow cell attachment, fresh medium was infused through the chamber to remove non-adhered cells. For immunostaining, cells were fixed with a 4 % paraformaldehyde (Alfa Aesar) solution in PBS for 15 min and then rinsed with PBS. After 15 min permeabilization with 0.1 % TritonX-100 (Sigma Aldrich) in PBS and 1 h blocking with 0.1 % TritonX-100 and 3 % bovine serum albumin (Sigma Aldrich) in PBS, focal adhesions and microtubules were stained simultaneously for 1 h using an anti-vinculin antibody (Sigma Aldrich, dilution 1/200) and an anti-β-tubulin antibody (Abcam, dilution 1/100), respectively. Anti-mouse-Alexa488 diluted 1/200 and anti-rabbit-Alexa647 diluted 1/100 (Jackson Immunoresearch) were used as secondary antibodies for focal adhesion and microtubule staining, respectively. F-actin and nuclei were stained respectively using phalloidin-Alexa-594 (Invitrogen, dilution 1/50) and DAPI (Invitrogen, dilution 1/100,000) during the secondary antibody 1 h incubation.

2.4 Image acquisition and quantification

Images were acquired on an inverted motorized microscope (Nikon Eclipse Ti-U) controlled by MicroManager (Edelstein et al. 2010) or NIS-Elements Advanced Research software and equipped with a CCD camera (Retiga; Q-imaging). Cell imaging was performed using either a 20× 0.5 NA dry objective or a 60× 1.40 NA oil immersion objective. For calcium imaging, BAECs were incubated for 30 min with 4 μM Fluo-4 AM (Invitrogen) in complete DMEM. Experiments started 15 min after extensive but gentle washing with DMEM. Images were acquired at one frame per second for 2 min. Individual cell fluorescence over time was quantified using ImageJ analysis software (Schneider et al. 2012) and normalized by the mean fluorescence of the first ten images acquired before flow application. For control calcium experiments using ionomycin, cells were cultured on a patterned or unpatterned coverslip placed in a petri dish (Chamlide) and exposed to 2 μM ionomycin (Sigma Aldrich) in complete DMEM. Data in all calcium experiments were analyzed using Excel and GraphPad Prism. For all movies, flow or ionomycin was applied only after acquisition of several reference (baseline) images. For lamellipodium visualization, phase contrast images were acquired every 30 s for 20 min. Temperature control during live-cell experiments was achieved using a heated stage plate (Warner Instruments), and pH buffering for longer-term imaging was enabled by using complete DMEM containing an extra 25 mM HEPES (50 mM total).

2.5 Micro particle image velocimetry

For micro particle image velocimetry (PIV), the perfusion fluid was seeded with 1 μm red fluorescent polymer microspheres (Thermo Scientific). Micro PIV was performed using a double-pulsed Nd:YAG laser frequency-doubled to 532 nm (Litron) for illumination, a double-frame CCD camera (LaVision) for image acquisition, and DaVis software for synchronization of laser and camera. A TRITC filter cube was used in combination with a 20× 0.5 NA dry objective to achieve high-resolution high-quality particle images. For each PIV run, 100 image pairs (approximately 400 × 400 pixels) were acquired with a 0.185 ms interframe time and analyzed using MATLAB-based open-source software (Prana). An advanced sum-of-correlation algorithm was used to obtain ensemble-averaged velocity fields (Meinhart et al. 1999; Eckstein and Vlachos 2009a; Eckstein and Vlachos 2009b).

3 Results and discussion

3.1 Endothelial cell shape is controlled using adhesive micropatterns

To control BAEC shape independently of flow, we used deep UV-generated adhesive micropatterns on a glass coverslip. This microfabrication technique has been used previously to geometrically confine various cell types including ECs (Chen et al. 1997; Anderson and Hinds 2011; Théry 2010). Compared to the micro-contact printing method, the deep

UV method used in this study allows more precise and reproducible control of micropattern fabrication (Fink et al. 2007; Azioune et al. 2009). As detailed in Methods, deep UV micropatterning consists of deposition of a cell-repellent molecule, PLL-g-PEG, onto the entire surface of a thin glass coverslip, followed by deep UV ablation of the molecule through a photomask in order to produce the desired micropatterns. The surface is subsequently coated with fibronectin, which fills in the UV-ablated zones to form the cell-adhesive micropatterns. This procedure creates a juxtaposition of cell-adhesive and cell-repulsive domains (Fig. 1).

To mimic the stereotypical elongated and oriented EC monolayer observed both *in vivo* and *in vitro* after long-term flow exposure (Levesque and Nerem 1985), we used adhesive stripes composed of 5 μm-wide adhesive lines spaced by 5 μm non-adhesive gaps. These small dimensions allowed individual ECs to bridge several adhesive lines, thus making cell-cell connections and forming monolayers, while at the same time confining sub-cellular structures such as focal adhesions to induce cellular elongation and alignment. On these surfaces, BAECs cultured at high density were highly oriented in the direction of the adhesive stripes, as was their filamentous actin (F-actin) cytoskeleton (Fig. 1 middle panel). On the contrary, BAECs cultured on unpatterned (control) surfaces produced a monolayer composed of randomly oriented cells (Fig. 1 left panel).

In addition to studying cellular monolayers, probing the responses of individual ECs provides important fundamental insight into cellular mechanotransduction. To this end, we also cultured BAECs on isolated 15 μm-wide adhesive lines spaced by 50 μm gaps. In this configuration, the adhesive lines were sufficiently wide to allow significant cell spreading within the line while the gap between lines was too large for cells to bridge multiple lines. Using this micropattern, we obtained highly elongated ECs oriented along the adhesive lines. By adjusting cell density, we were able to obtain completely isolated cells or individual cells with few neighbors (Fig. 1 right panel).

The results above demonstrate that by using adhesive micropatterns we are able to control EC elongation and orientation at both the monolayer and single cell levels without application of flow. In the course of these studies, we noticed that individual ECs cultured on isolated 15 μm-wide lines were often highly polarized, with a large lamellipodium at one extremity and a prominent contractile rear composed of actin stress fibers at the other extremity (Fig. 1 and Fig. 2d), resembling the typical polarization of a migratory cell (Michaelis 2014). As will be elaborated upon later, this particular feature yields the opportunity to study the interplay between EC polarization and mechanotransduction.

3.2 Endothelial cell polarization in the flow chamber

Using the adhesive micropatterns, we controlled EC shape and orientation independently of flow. To expose ECs to a controlled level of flow-derived shear stress, we used the micropatterned coverslip (or an unpatterned coverslip in control experiments) as one of the surfaces of a parallel plate microfluidic flow chamber as described above in Methods. The thin glass micropatterned surface enabled high-resolution live-cell imaging. As indicated in Methods, the microfluidic flow chamber is assembled together using double-sided tape (Fig. 2a). The chamber combines the advantages of imaging the sample through a thin (~150 μm) glass coverslip with the convenience of handling a sturdy device due to the microscope slide top surface (Fig. 2b). The flow channel between the two surfaces is simply cut into the double-sided tape to create an 18.5 × 30-mm channel, sufficiently large to provide a wide selection of cellular regions of interest. The height of the chamber is defined by the thickness of the double-sided tape, which was measured by profilometry

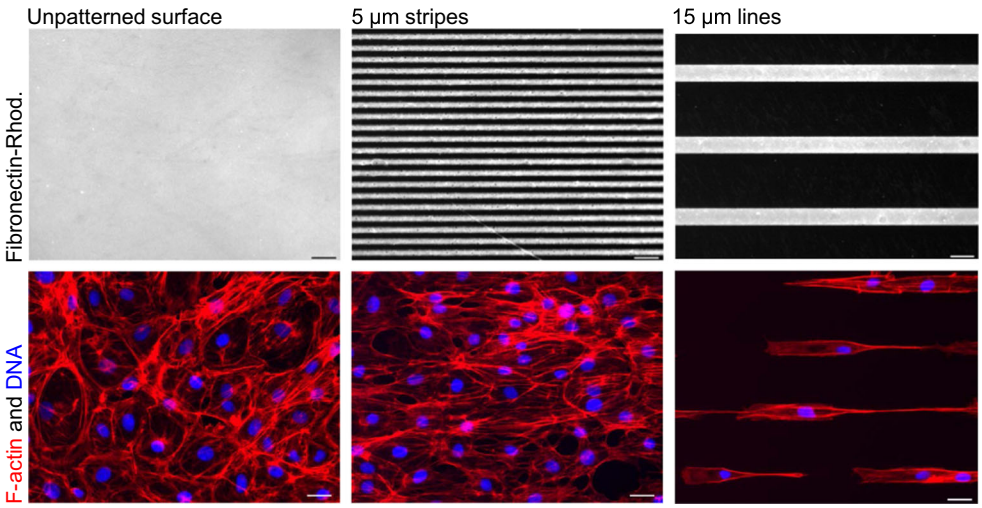

Fig. 1 Control of EC shape by adhesive micropatterning at either the monolayer or single cell level. Top row: Localization of fluorescent fibronectin on an unpatterned surface (*left*), on 5 μm stripes (*middle*) and on isolated 15 μm lines (*right*). Bottom row: Immunostained BAECs cultured under static conditions on the micropatterned surfaces described above. F-actin (*red*) is stained with phalloidin and nuclei (*blue*) with DAPI. Scale bars are 20 μm

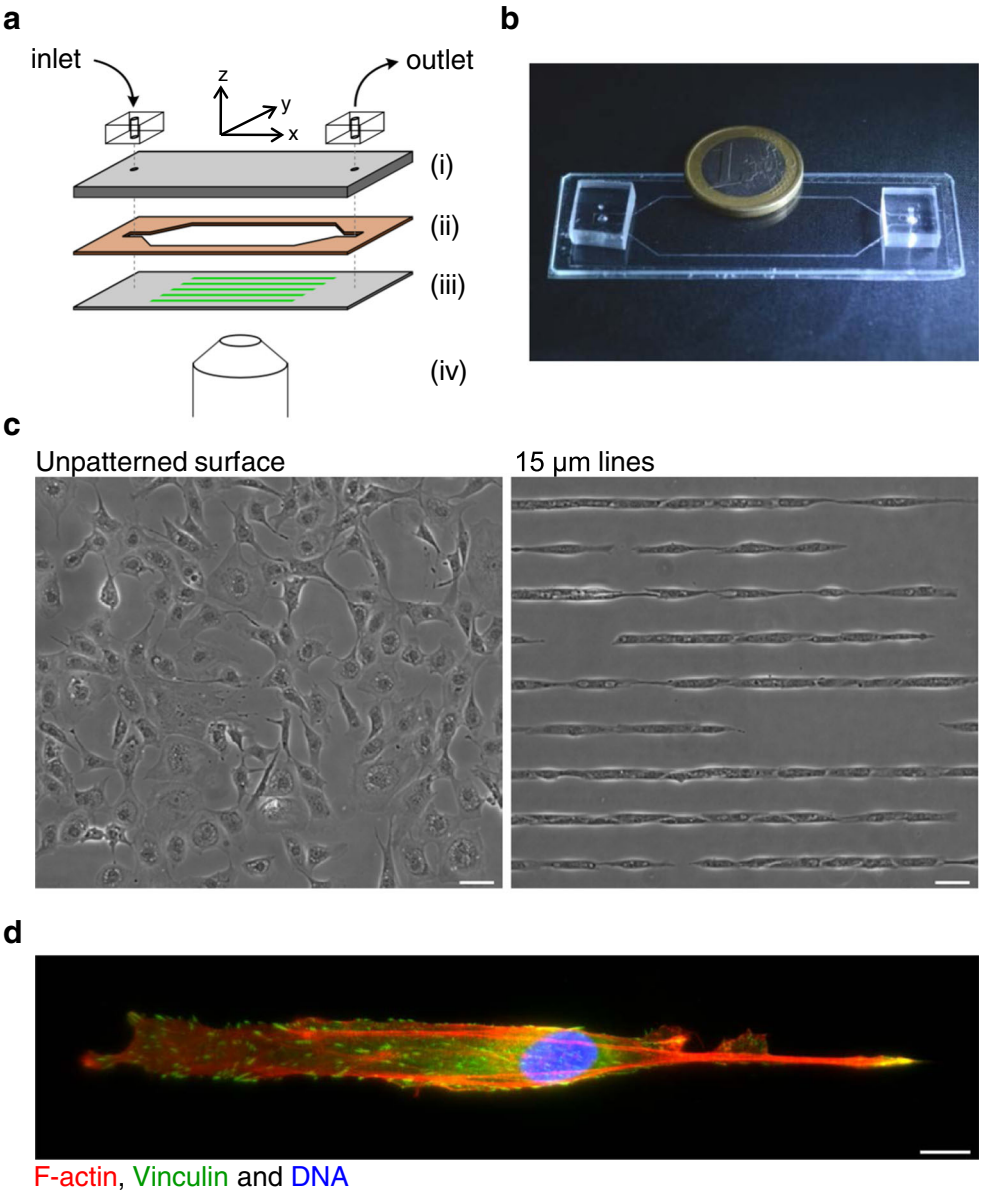

Fig. 2 BAEC shape controlled by adhesive micropatterning in a microfluidic chamber. (**a**) Design of the microfluidic chamber. i) Regular microscope glass slide (25 × 75 mm, 1 mm thick). ii) Double-sided adhesive tape (100 μm thick). iii) Micropatterned glass coverslip (~150 μm thick). iv) High numerical aperture microscope objective. (**b**) Photograph of the microfluidic chamber. (**c**) Phase contrast images of BAECs cultured under static conditions in the microfluidic chamber containing either an unpatterned surface (left panel) or isolated 15 μm adhesive lines (right panel). Scale bars are 50 μm. (**d**) Immunostaining of an EC cultured under static conditions in the microfluidic chamber containing isolated 15 μm adhesive lines. F-actin (*red*) is stained with phalloidin, focal adhesions (*green*) with an anti-vinculin antibody, and nucleus (*blue*) with DAPI. Scale bar is 10 μm. Additional immunostaining is shown in Fig. S1

to be 100 μm. Note that production of the microfluidic chamber does not require photolithography.

In the microfluidic chamber, BAECs cultured under static conditions on isolated 15 μm adhesive lines were highly elongated and oriented in the direction of the micropatterns (Fig. 2c right panel) compared to control cells cultured under the same conditions on an unpatterned surface (Fig. 2c left panel). Immunostaining was performed directly in the chamber without requiring disassembly of the system by perfusing fixation and staining solutions through the chamber. To demonstrate this capability, the highly polarized state of ECs cultured on isolated 15 μm lines was visualized by staining various intracellular structures (Fig. 2d and Online resources Fig. S1) including actin filaments (phalloidin), focal adhesions (vinculin), the nucleus (DAPI), and microtubules (β-tubulin). The staining revealed a wide lamellipodium at the front of the cell which contained a dense actin meshwork and long mature focal adhesions, whereas the rear of the cell contained prominent actin stress fibers and fewer focal adhesions, typical of a retracting cellular end. The nucleus was positioned between the contractile rear and the lamellipodium, while the position of the microtubule organizing center, determined by microtubule staining (Fig. S1), was in front of the nucleus (i.e. on the lamellipodium side of the nucleus).

3.3 Wall shear stress measurements using micro particle image velocimetry

Next, we quantified the local shear stress experienced by ECs while under flow. As the microfluidic chamber allows high-

quality videomicroscopy, we were able to measure the flow field in multiple z-planes over the cells using micro PIV (a complete review of the technique can be found elsewhere (Lindken et al. 2009)). In chambers containing BAECs adhered to either an unpatterned surface or to isolated 15 μm lines, we performed micro PIV image acquisition in a centered region of interest. We measured both the axial (x) and transverse (y) fluid velocity components U and V in four different z-planes over the ECs, from 0 to 13 μm (Fig. S2a), obtaining 2400 vectors per slice with a resolution of 2.96 μm/vector. The wall shear stress was then computed by multiplying the axial velocity gradient at the wall (dU/dz) by the dynamic viscosity of the fluid (0.94×10^{-3} Pa*s for DMEM at 25 °C (Fröhlich et al. 2013)) at each vector position. The velocity gradient was estimated from a linear fit to the four velocity measurements corresponding to the four z-planes (Fig. S2b). In parabolic flow, the assumption of linearity introduces no more than 10 % error for measurements within 0.1 diameters of the wall. Although the z = 0 plane was not exactly coincident with the coverslip surface, the slope estimate is invariant to this error in the near-wall region. By averaging the wall shear stress measured over all 2400 grid positions, we obtained an estimated average wall shear stress of 0.63 ± 0.035 Pa (6.3 ± 0.35 dyn/cm^2; mean ± SD) for unpatterned cells and 0.57 ± 0.039 Pa (5.7 ± 0.39 dyn/cm^2) for ECs confined to 15 μm lines.

Given the dimensions of the flow chamber, one can estimate shear stress at the wall based on an approximation of steady flow between two infinitely wide parallel plates (Poiseuille flow). In this case, the shear stress at the wall is given by: $WSS = (6\mu Q)/(h^2 w)$ where Q is the volumetric flow rate applied to the chamber, μ the dynamic viscosity of the fluid, h the height of the chamber, and w the width of the chamber. Based on this expression, the expected wall shear stress in a chamber with Q = 1.8 mL/min, w = 18.5 mm, h = 100 μm and $\mu = 0.94 \times 10^{-3}$ Pa*s is 0.91 Pa (9.1 dyn/cm^2). The mean shear stresses measured by micro PIV were thus significantly lower than this prediction. We attribute this discrepancy to non-negligible swelling of the chamber caused by the increased static pressure during perfusion. Using the microscope motorization, we measured the mean height of the microfluidic chamber during flow perfusion and found it to be 142 μm instead of the expected 100 μm. Based on the measured chamber height, the shear stress is expected to be 0.45 Pa (4.5 dyn/cm^2) which is more consistent with the PIV-measured shear stresses. This illustrates the importance of measuring the shear stress in this and similar microfluidic devices rather than simply estimating it based on nominal dimensions. Using this validation of our microfluidic system design and flow setup, we can in the future apply a controlled physiologically relevant shear stress to ECs cultured on adhesive micropatterns.

3.4 Endothelial cell shape affects local cell-scale shear stress

In addition to measuring mean shear stresses to validate the microfluidic chamber, we investigated whether the flow field and local shear stress perceived by the cells were affected by EC shape. We first analyzed ECs cultured in a chamber containing an unpatterned surface (Fig. 3a top row). The wall shear stress map overlaid with the phase contrast image of the cells indicates high correlation between zones of higher shear stress and zones containing cells (right panel). Indeed, we were able to quantify this effect by grouping wall shear stress measurements based on different regions identified in the phase contrast images. We observed that the shear stress over the cells was significantly higher (4.1 %) than the shear stress in regions containing no cells. Moreover, we observed an even larger difference between shear stresses over cell nuclei compared to regions containing no cells (5.4 %). For the experiment with ECs cultured in a microfluidic chamber containing 15 μm lines oriented parallel to the flow direction (Fig. 3a bottom row), we again observed a higher shear stress over the cells compared to regions containing no cells (5.8 %). Finally, shear stresses over the nuclei of cells parallel to flow showed the most significant increase of all the cases analyzed, with a mean value 12.9 % higher than in regions containing no cells. All the presented comparisons were found to be highly statistically significant with $p < 0.001$ using a two-way ANOVA analysis with Tukey's multiple comparison post-hoc test.

The influence of the patterned cells on the near-cell flow field can further be seen in contour maps of the axial and transverse components of the velocity (U and V respectively, Fig. 3b). While the U component across each cell is merely reduced, the V component shows flow diversion around each cell. This is evidenced by paired positive/negative regions in the V component in the upstream and downstream halves of the cell; see, for example, the cell highlighted in the figure with the accompanying schematic of the flow behavior. These results demonstrate that our system is able to measure cell-scale shear stresses and establish that the local shear stress is affected by EC shape. Because cell biological responses to flow are expected to be determined by the shear stress perceived by the cells at the local level, the ability to measure cell-scale shear stress as demonstrated here is critical for understanding EC mechanotransduction.

3.5 Cell polarization in response to flow application

An important EC response to flow is cell polarization and migration in the direction of the flow (Morgan et al. 2012). To verify that ECs were responsive to flow in our microfluidic chamber, we imaged cells for 30 min after flow initiation (steady flow at 1.8 mL/min) in order to detect flow-induced

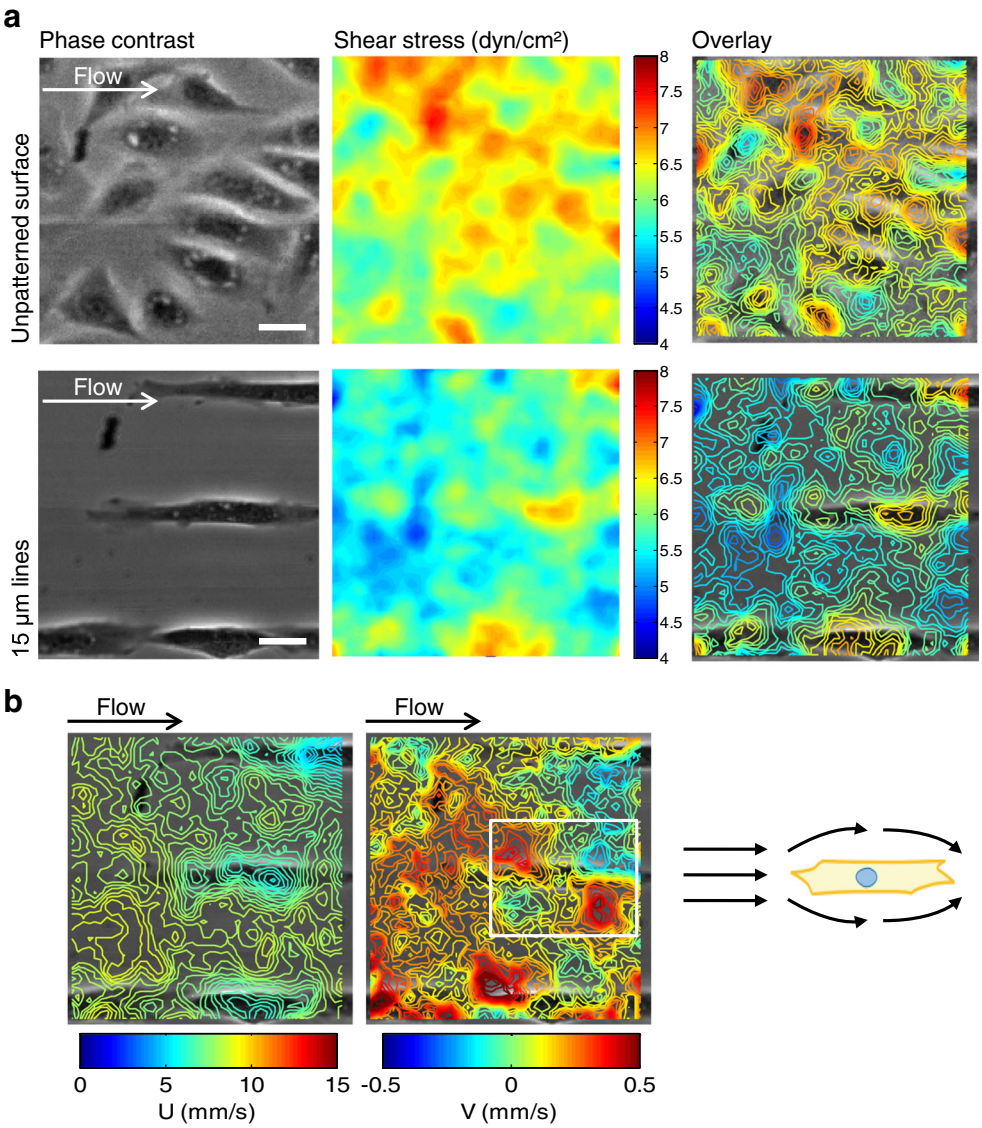

Fig. 3 Cell-scale shear stress measurements using micro particle image velocimetry (PIV). (**a**) BAECs cultured in the microfluidic chamber whose bottom surface consisted of either an unpatterned coverslip (*top row*) or a coverslip patterned with isolated 15 μm adhesive lines (*bottom row*). Left panels: phase contrast images of the cells in the chamber during micro PIV measurements. Scale bars are 25 μm and arrows denote the direction of flow. Middle panels: map of wall shear stresses at each grid location. Right panels: overlay between the phase contrast image and the color contour of wall shear stress. Note the correlation between zones of high shear stress and regions containing cells. (**b**) Color contours of axial velocity component U (left panel) and transverse velocity component V (right panel) at z = 3.3 μm for the microfluidic chamber containing isolated 15 μm adhesive lines. Note the different scaling for U and V. The schematic depicts the flow deviation around the cell observed in the white box

EC polarization. Our system allowed us to visualize structures such as lamellipodia and cell contraction zones using high-resolution phase contrast imaging. This experiment was performed on BAECs cultured in a microfluidic chamber with an unpatterned bottom surface (Fig. 4 and Online resources Movie S1). After less than 20 min of flow, we observed the formation of large lamellipodia at the downstream ends of several cells (arrow heads) as well as cell rear retraction at the upstream ends (arrows). The overlay of cell contours before and after flow (Fig. 4 bottom right panel) highlights this flow-induced cellular polarization response.

3.6 Calcium mobilization upon flow application

Another important EC response to flow is calcium mobilization (Ando and Yamamoto 2013); however, studies to date of this response have only been performed on unpatterned surfaces where cells take on many different shapes and orientations. To explore if the calcium response also occurs in ECs cultured on micropatterned surfaces where cell shape and orientation are highly regulated, we performed high-resolution calcium imaging of BAECs cultured in a microfluidic chamber containing an unpatterned surface or isolated 15 μm adhesive lines oriented either parallel or orthogonal to the flow (Fig. 5a, left, middle, and right panels, respectively). Changes in intracellular calcium were monitored using the calcium-sensitive fluorescent probe Fluo-4 AM at a relatively fast acquisition rate (1 Hz). Basal fluorescence of the cells was recorded for 15 s before flow application, and the cells were imaged for 2 min after flow application with the same flow conditions as those used above, i.e. steady flow rate of 1.8 mL/min (Movie S2).

Individual cell fluorescence was quantified over time and normalized by the mean fluorescence of 10 images acquired

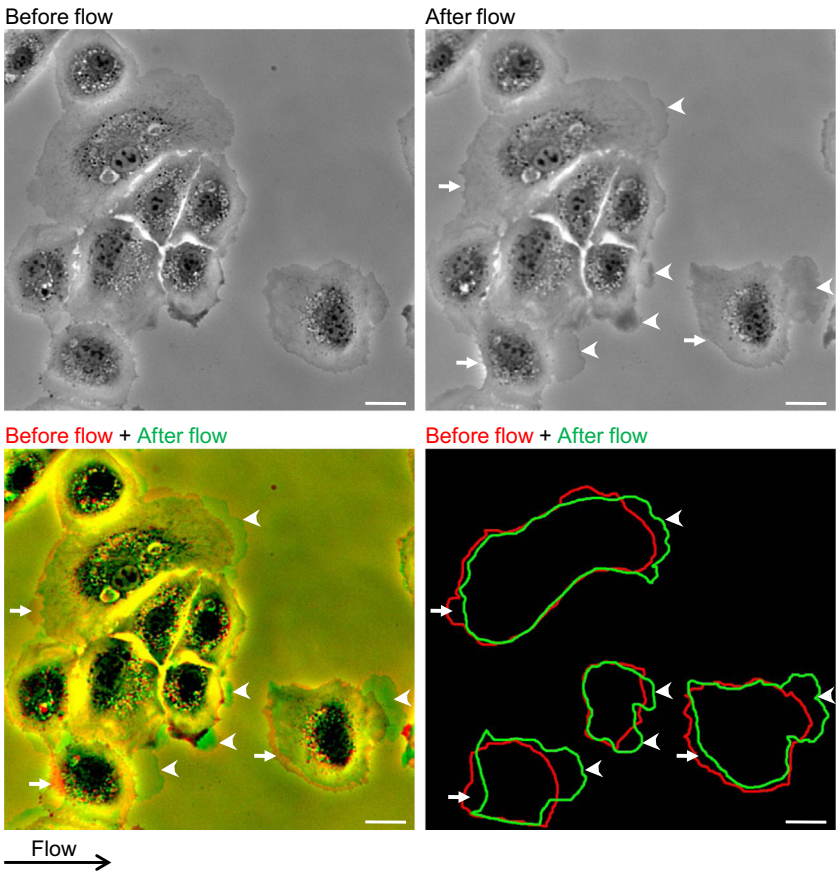

Fig. 4 Flow-induced cell polarization. Phase contrast images of BAECs cultured in a microfluidic chamber containing an unpatterned surface before flow application (*top left*) and after 17 min of flow (*top right*). The bottom left panel is an overlay of the before (*red*) and after (*green*) phase contrast images, and the bottom right panel represents the hand-drawn individual cell contours. Arrowheads indicate lamellipodium extension and arrows show cell rear contraction. Flow is from left to right. Scale bars are 20 μm

immediately before flow application. The recordings revealed significant heterogeneity among cells with the overall response described by two distinct groups of cells: 'Group 1' exhibitied a robust calcium response while 'Group 2' showed only minimal changes in intracellular calcium levels. Based on the results, Group 1 cells were defined as those exhibiting a maximum fluorescence intensity during flow that is ≥1.3 times the pre-flow basal intensity. Defining this cutoff provided a clear separation between the two groups. As a positive control, we challenged cells cultured on either an unpatterned surface or on isolated 15 μm adhesive lines (Fig. S3a) with ionomycin (2 μM). The cells exhibited a strong calcium response uniformly and did not show the two-group separation observed under flow (Fig. S3b).

As depicted in Fig. 5b, the intracellular calcium response to flow was transient; it initiated ~5–10 s after flow onset, peaked at ~15–20 s, and then decreased gradually back to the pre-flow basal level at ~50–60 s. This behavior was similar for cells cultured on either an unpatterned surface or on 15 μm adhesive lines oriented parallel or orthogonal to the flow. Nevertheless, we noticed a difference in the proportion of cells belonging to Group 1 or Group 2 among the different surfaces (Fig. S4a). More specifically, cells cultured in a microfluidic chamber with isolated 15 μm lines oriented orthogonal to the flow exhibited a higher percentage of Group 1 cells (66 %) compared to cells cultured in the chamber with isolated 15 μm adhesive lines oriented parallel to the flow (55 %) and cells cultured in the chamber with an unpatterned surface (40 %). Moreover, the Group 1 cells on 15 μm lines orthogonal to the flow presented a sharper calcium response compared to the two other conditions (Fig. S4b red curve). Taken together, these results suggest heightened calcium sensitivity to flow in BAECs cultured on 15 μm lines, especially when the patterned surface (and hence the cell major axis) is oriented orthogonal to the flow.

3.7 Intracellular calcium wave propagation is determined by cellular polarization

In addition to overall calcium mobilization, we observed in some cells intracellular calcium waves after flow application. In these cases, the increase in fluorescence triggered by the flow application was first observed at one localized subcellular site in the cell, then propagated to the rest of the cell in a given direction (Fig. 6a and Movie S3). Because flow application is intrinsically directional, we hypothesized that the direction of the calcium wave observed in the cells may be dictated by the direction of the flow. To test this idea, we quantified the direction of the flow-induced calcium wave propagation relative to the direction of the flow (taken as

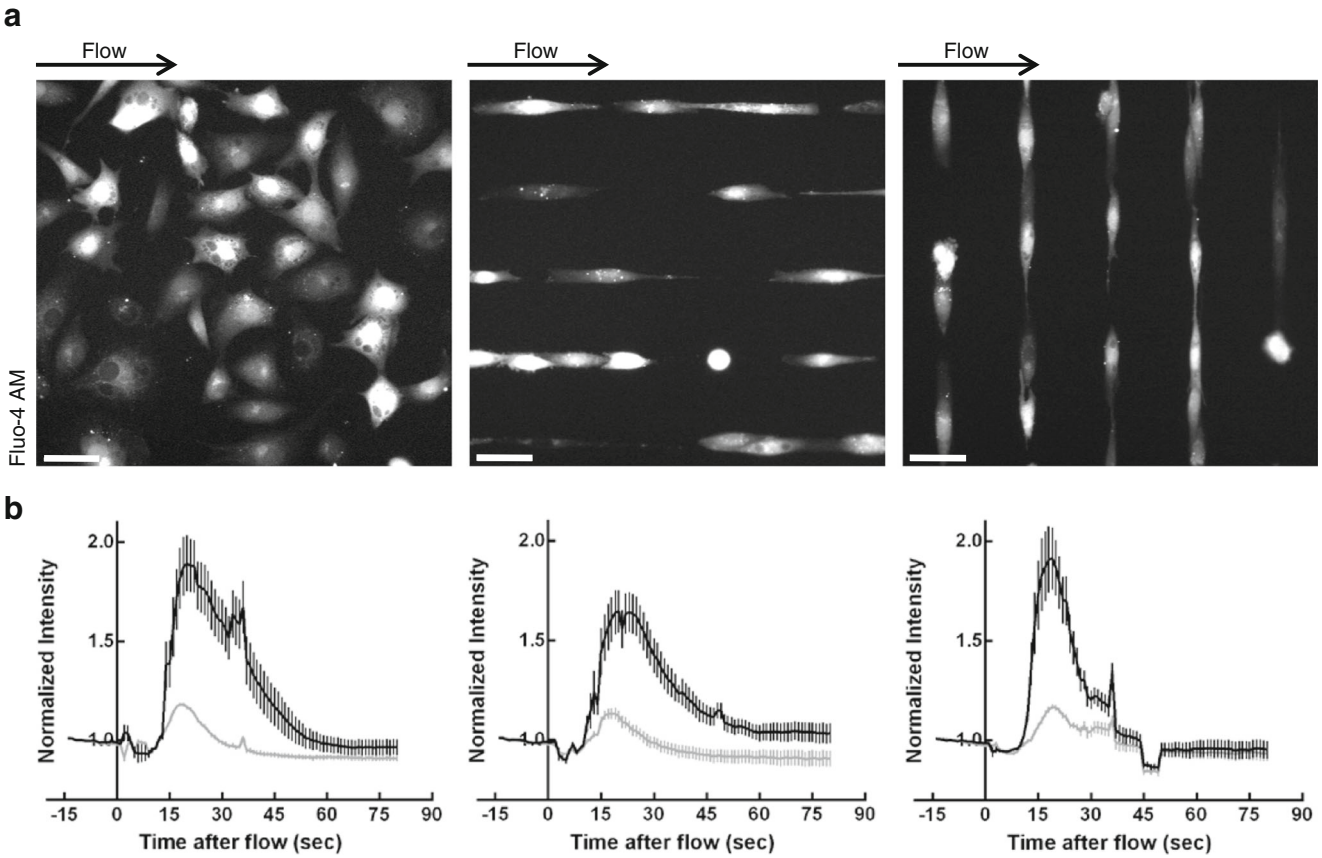

Fig. 5 Intracellular calcium mobilization in BAECs upon flow application. (**a**) Representative image of the fluorescent signal obtained using the calcium probe Fluo-4 AM in BAECs cultured in the microfluidic chamber containing an unpatterned surface (*left*) or isolated 15 μm adhesive lines oriented either parallel (*middle*) or orthogonal (*right*) to the flow. Scale bar is 40 μm. (**b**) Quantification of individual cell fluorescence over time from 3 independent experiments, $n = 83$ for unpatterned surface, $n = 38$ for parallel and $n = 47$ for orthogonal. The black curves represent the mean of Group 1 cells, while the grey curves represent the mean of Group 2 cells; the bars represent the standard error of the mean

0°). In all the experiments combined, we did not observe any favored wave angle (Fig. 6b), suggesting that the flow direction does not determine the direction of propagation of the intracellular calcium wave.

We then asked if the polarization of the cells could direct the intracellular calcium waves. To address this question, we focused on cells cultured on micropatterned surfaces in which the cell polarization is well controlled and quantifiable compared to the highly complex and difficult to characterize polarization of cells cultured on unpatterned surfaces. In these confined cells, the polarization angle is defined as the angle between the rear-front axis of the cell and the flow direction. Because of the design of the experiments, the only possible cell polarization angles are 0° and 180° for cells cultured on 15 μm lines oriented parallel to the flow, and 90° and 270° for cells cultured on 15 μm lines oriented orthogonal to the flow. In these two types of experiments (12 cells), we always observed the calcium wave starting at the cell rear and propagating to the cell front, independently of the flow direction. We obtained this correlation between the calcium wave angle and the cell polarization angle (Fig. 6c) even in the extreme case where the calcium wave propagated opposite to the flow direction (180°). These results demonstrate that the intracellular calcium wave direction is dictated by the cell polarization rather than the flow direction.

Intracellular calcium waves have previously been observed in ECs and correlated to ATP release from caveolae-rich regions (Yamamoto et al. 2011). As caveolae are associated with actin microfilaments (Richter et al. 2008; Parton and del Pozo 2013), we speculate that the strong polarization of actin in ECs cultured on 15 μm lines polarizes caveolar localization, thus orienting intracellular calcium waves. This idea merits future study.

4 Conclusions

In this work, we have presented a simple microfluidic device to study the interplay between cell shape and responsiveness to flow. Thanks to a combination of robust fabrication and imaging tools, we have succeeded in independently

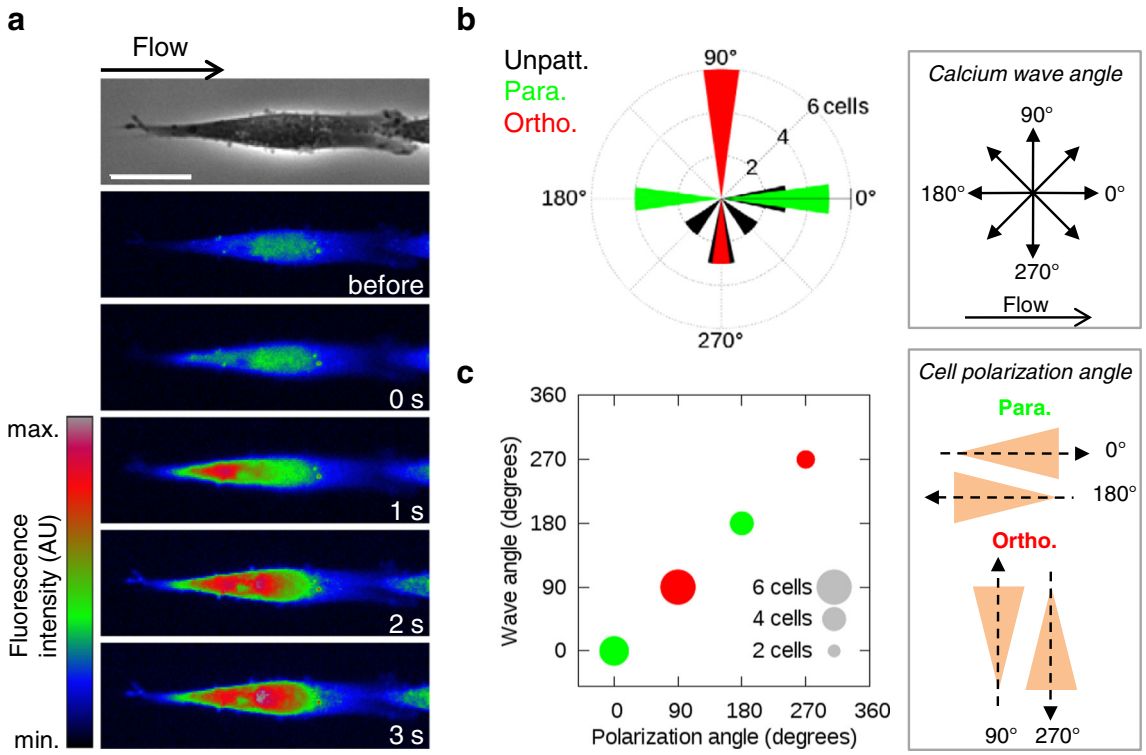

Fig. 6 Intracellular calcium waves after flow application. (**a**) Individual EC cultured in the microfluidic chamber containing 15 μm adhesive lines oriented parallel to the flow. From top to bottom, the first panel is a phase contrast image of the cell; the others are color-coded fluorescence intensity (in arbitrary units AU) images. Time is labeled in seconds after the beginning of the wave. Scale bar is 20 μm. (**b**) Quantification of calcium wave angles in cells cultured in the microfluidic chamber with an unpatterned surface (*black*), parallel micropatterns (*green*), or orthogonal micropatterns (*red*). (**c**) Calcium wave angle as a function of cell polarization angle for cells cultured on parallel (*green*) and orthogonal (*red*) micropatterns

controlling EC shape and applying controlled shear stresses while dynamically following EC mechanotransduction events.

UV micropatterning permits highly reproducible surface patterns at both the monolayer and single cell levels. Flow application was achieved using a microfluidic chamber which is easily implemented due to the simplicity of its fabrication and its ease of use. Importantly, the system allows high-resolution live-cell imaging in both phase contrast and fluorescence, enabling quantification of real-time EC responses to flow. We used micro PIV to characterize the global wall shear stress in the chamber as well as the local cell-scale shear stress experienced by individual micropatterned ECs. We measured significantly higher shear stresses over cell nuclei compared to regions containing no cells, suggesting that cells alter the local flow field to which they are subjected. We performed high-resolution phase contrast videomicroscopy to track flow-induced EC polarization. Lamellipodium formation was observed at the downstream end of the cell and cell retraction at the upstream end. We quantified the global flow-induced calcium mobilization in individual ECs cultured on an unpatterned surface or on isolated 15 μm adhesive lines oriented either parallel or orthogonal to the flow. We observed largely similar responses among the three groups in terms of the dynamics and average intensity of calcium mobilization; however, the fraction of cells exhibiting a strong calcium response was highest for cells cultured on patterned surfaces oriented orthogonal to the flow. Lastly, our imaging system allowed us to perform fluorescent live-cell imaging with a subcellular resolution. We detected intracellular calcium waves whose direction of propagation was determined by the cell polarization direction rather than by the flow direction. Whenever they occurred, the calcium waves always started at the cell rear and propagated to the cell front within a few seconds.

In conclusion, the microfluidic device described here provides a simple but robust tool for addressing crucial unanswered questions in EC flow-mediated mechanotransduction. In particular, the control of EC shape combined with cell-scale shear stress measurements can produce new insight into how EC shape affects the flow field and how the resulting modification of cell-scale shear stress regulates EC responses to flow-derived forces. UV adhesive micropatterning is a highly versatile tool and can be used to control many cell parameters such as cell orientation relative to the flow, the extent of cell elongation, and even sub-cellular polarization of intracellular components (Théry et al. 2006). As cell shape and flow are independently controlled in the device, the orientation

between cells and flow-derived forces can be modulated as desired. By varying cell density in the system described here, the number of neighbors with which a cell interacts can be controlled, thus permitting the investigation of the role of cell-cell contact within a group of cells or a monolayer. Finally, an interesting feature of the device is the ability to combine live-cell imaging during flow with immunostaining directly in the chamber immediately after flow in order to perform correlative analysis. Because certain intracellular components can only be visualized using immunostaining on fixed samples (using standard or super-resolution imaging) while others are amenable to live-cell probes, this type of correlative analysis offers the possibility to decipher molecular mechanisms of EC mechanotransduction.

Acknowledgments The authors thank Bertrand Levaché for introducing them to the double-sided tape microfabrication technique and Maria Isabella Gariboldi for her participation in micropatterning technique development. This work was supported in part by an endowment in cardiovascular cellular engineering from the AXA Research Fund. Julie Lafaurie-Janvore was funded by postdoctoral fellowships from the Fondation Lefoulon-Delalande and the AXA Research Fund. Elizabeth Antoine was funded by a Whitaker International Program postdoctoral fellowship. Sidney J. Perkins was supported by a summer research international student fellowship from École polytechnique and the Columbia University European Institute's Fellowship Program.

References

F. An, Q. Yueyang, X. Liu, R. Zhong, Y. Luo, Organ-on-a-Chip: new platform for biological analysis. Anal. Chem. Insights. **10**, 39–45 (2015)

D. E. J. Anderson, M. T. Hinds, Endothelial cell micropatterning: methods, effects, and applications. Ann. Biomed. Eng. **39**(9), 2329–2345 (2011)

J. Ando, K. Yamamoto, Flow detection and calcium Signalling in vascular endothelial cells. Cardiovasc. Res. **99**(2), 260–268 (2013)

A. Azioune, M. Storch, M. Bornens, M. Théry, M. Piel, Simple and rapid process for single cell micro-patterning. Lab Chip **9**(11), 1640–1642 (2009)

A. Azioune, N. Carpi, Q. Tseng, M. Théry, M. Piel, Protein micropatterns: a direct printing protocol using deep UVs. Methods Cell Biol. **97**, 133–146 (2010)

A. I. Barakat, Blood flow and arterial endothelial dysfunction: mechanisms and implications. C. R. Physique **14**, 479–496 (2013)

K. A. Barbee, T. Mundel, R. Lal, P. F. Davies, Subcellular distribution of shear stress at the surface of flow-aligned and nonaligned endothelial monolayers. Am. J. Physiol. Heart Circ. Physiol. **268**, H1765–H1772 (1995)

D. J. Beebe, D. E. Ingber, J. Den Toonder, Organs on chips 2013. Lab. Chip. **13**, 3447–3448 (2013)

J. M. Chan, K. H. K. Wong, A. M. Richards, C. L. Drum, Microengineering in cardiovascular research: new developments and translational applications. Cardiovasc. Res. **106**, 9–18 (2015)

Y. S. Chatzizisis, A. U. Coskun, M. Jonas, E. R. Edelman, C. L. Feldman, P. H. Stone, Role of endothelial shear stress in the natural history of coronary atherosclerosis and vascular remodeling: molecular, cellular, and vascular behavior. J. Am. Coll. Cardiol. **49**(25), 2379–2393 (2007)

C. S. Chen, M. Mrksich, S. Huang, G. M. Whitesides, D. E. Ingber, Geometric control of cell life and death. Science. **276**(5317), 1425–1428 (1997)

S. Chien, Mechanotransduction and endothelial cell homeostasis: the wisdom of the cell. Am. J. Physiol. Heart Circ. Physiol. **292**, 1209–1224 (2007)

P. F. Davies, Flow-mediated endothelial mechanotransduction. Physiol. Rev. **75**(3), 519–560 (1995)

N. DePaola, P. F. Davies, W. F. Pritchard, L. Florez, N. Harbeck, D. C. Polacek, Spatial and temporal regulation of gap junction connexin43 in vascular endothelial cells exposed to controlled disturbed flows in vitro. Proc. Natl. Acad. Sci. **96**, 3154–3159 (1999)

A. Eckstein, P. P. Vlachos, Assessment of advanced windowing techniques for digital particle image velocimetry (DPIV). Meas. Sci. Technol. **20**, 075402 (2009a)

A. Eckstein, P. P. Vlachos, Digital particle image velocimetry (DPIV) robust phase correlation. Meas. Sci. Technol. **20**, 055401 (2009b)

A. Edelstein, N. Amodaj, K. Hoover, R. Vale, N. Stuurman, Computer control of microscopes using μManager. Curr. Protoc. Mol. Biol. Chapter **14**, 14.20.1–14.20.17 (2010)

J. Fink, M. Théry, A. Azioune, R. Dupont, F. Chatelain, M. Bornens, M. Piel, Comparative study and improvement of current cell micropatterning techniques. Lab. Chip. **7**(6), 672–680 (2007)

E. Fröhlich, G. Bonstingl, A. Höfler, C. Meindl, G. Leitinger, T. R. Pieber, E. Roblegg, Comparison of two *in vitro* systems to assess cellular effects of nanoparticles-containing aerosols. Toxicol. *in Vitro.* **27**(1), 409–417 (2013)

C. L. M. Gouget, Y. Hwang, A. I. Barakat, Model of cellular mechanotransduction via actin stress fibers. Biomech. Model. Mechanobiol Springer Berlin Heidelberg **15**, 331–344 (2015)

C. Hahn, M. A. Schwartz, Mechanotransduction in vascular physiology and Atherogenesis. Nat. Rev. Mol. Cell Biol. **10**(1), 53–62 (2009)

S. Hsu, R. Thakar, D. Liepmann, S. Li, Effects of shear stress on endothelial cell Haptotaxis on micropatterned surfaces. Biochem. Biophys. Res. Commun. **337**(1), 401–409 (2005)

R. H. W. Lam, Y. Sun, W. Chen, F. Jianping, Elastomeric Microposts integrated into microfluidics for flow-mediated endothelial mechanotransduction analysis. Lab. Chip. **12**(10), 1865–1873 (2014)

M. J. Levesque, R. M. Nerem, The elongation and orientation of cultured endothelial cells in response to shear stress. J. Biomech. Eng. **107**(4), 341–347 (1985)

Y.-S. J. Li, J. H. Haga, S. Chien, Molecular basis of the effects of shear stress on vascular endothelial cells. J. Biomech. **38**(10), 1949–1971 (2005)

X. Lin, B. P. Helmke, Cell structure controls endothelial cell migration under fluid shear stress. Cell. Mol. Bioeng. **2**(2), 231–243 (2012)

R. Lindken, M. Rossi, S. Grosse, J. Westerweel, Micro-particle image velocimetry (microPIV): recent developments, applications, and guidelines. Lab. Chip. **9**(17), 2551–2567 (2009)

C. D. Meinhart, S. T. Wereley, J. G. Santiago, PIV measurements of a microchannel flow. Exp. Fluids **27**, 414–419 (1999)

U. R. Michaelis, Mechanisms of endothelial cell migration. Cell. Mol. Life Sci. **71**(21), 4131–4148 (2014)

J. T. Morgan, J. A. Wood, N. M. Shah, M. L. Hughbanks, P. Russell, A. I. Barakat, C. J. Murphy, Integration of Basal Topographic Cues and Apical Shear Stress in Vascular Endothelial Cells. Biomaterials. **33**(16) Elsevier Ltd, 4126–4135 (2012)

R. G. Parton, M. A. del Pozo, Caveolae as Plasma Membrane Sensors, Protectors and Organizers. Nat. Rev. Mol. Cell. Biol. **14**(2) Nature Publishing Group, 98–112 (2013)

W. J. Polacheck, R. Li, S. G. M. Uzel, R. D. Kamm, Microfluidic platforms for mechanobiology. Lab. Chip. **13**(12), 2252–2267 (2013)

T. Richter, M. Floetenmeyer, C. Ferguson, J. Galea, J. Goh, M. R. Lindsay, G. P. Morgan, B. J. Marsh, R. G. Parton, High-resolution

3D quantitative analysis of caveolar ultrastructure and Caveola – cytoskeleton interactions. Traffic. **9**(29), 893–909 (2008)

R. L. Satcher, S. R. Bussolari, M. A. Gimbrone, C. F. Dewey, The distribution of fluid forces on model arterial endothelium using computational fluid dynamics. J. Biomech. Eng. **114**, 309–316 (1992)

C. A. Schneider, W. S. Rasband, K. W. Eliceiri, NIH image to ImageJ: 25 Years of image analysis. Nat. Methods. **9**, 671–675 (2012)

J. Shemesh, I. Jalilian, A. Shi, G. H. Yeoh, T. M. L. Knothe, M. E. Warkiani, Flow-induced stress on adherent cells in microfluidic devices. Lab .Chip. Royal Society of Chemistry (2015). doi:10.1039/C5LC00633C

M. Théry, Micropatterning as a tool to decipher cell morphogenesis and functions. J. Cell Sci. **123**(Pt 24), 4201–4213 (2010)

M. Théry, V. Racine, M. Piel, A. Pépin, A. Dimitrov, Y. Chen, J.-B. Sibarita, M. Bornens, Anisotropy of cell adhesive microenvironment governs cell internal organization and orientation of polarity. Proc. Natl. Acad. Sci. **103**(52), 19771–19776 (2006)

L. Wang, Z.-L. Zhang, J. Wdzieczak-Bakala, D.-W. Pang, J. Liu, Y. Chen, Patterning cells and shear flow conditions: convenient observation of endothelial cell Remoulding, enhanced production of angiogenesis factors and drug response. Lab. Chip. **11**(24), 4235–4240 (2011)

K. Yamamoto, K. Furuya, M. Nakamura, E. Kobatake, M. Sokabe, J. Ando, Visualization of flow-induced ATP release and triggering of Ca2+ waves at caveolae in vascular endothelial cells. J. Cell Sci. **124**(Pt 20), 3477–3483 (2011)

E. W. K. Young, C. A. Simmons, Macro- and microscale fluid flow Systems for Endothelial Cell Biology. Lab. Chip. **10**(2), 143–160 (2010)

A. Yurdagul, A. C. Finney, M. D. Woolard, A. W. Orr, The arterial microenvironment: the where and why of atherosclerosis. Biochem. J. **473**, 1281–1295 (2016)